Model Predictive Control for a Multi-Body Slung-Load System[☆]

Gaetano Tartaglione[a], Egidio D'Amato[b], Marco Ariola[a], Pierluigi Salvo Rossi[c], Tor Arne Johansen[d]

[a] *Department of Engineering, University of Naples Parthenope, Napoli, Italia*
[b] *Department of Industrial and Information Engineering, Second University of Naples, Aversa, Italy*
[c] *Department of Electronic Systems, Norwegian University of Science and Technology, Trondheim, Norway*
[d] *Center for Autonomous Marine Operation and Systems, Norwegian University of Science and Technology, Trondheim, Norway*

Abstract

In this paper we present a multi-level and distributed control system, based on a robust Model Predictive Control (MPC) technique, for a multi-body slung-load system. In particular, we consider a swarm of autonomous multi-copters which are connected by wires to a suspended payload. The payload reference trajectory is obtained through a constrained optimization, then the reference trajectory for each UAV is derived on the basis of the known shape of the formation, while taking into account operational constraints such as collision avoidance and cruise speed. Trajectory tracking is performed by a multi-level flight control system based on a MPC technique and a PID control system. Numerical simulations have been performed in order to test the control system in realistic scenarios. In particular, the multi-copters are modeled by the six Degrees-of-Freedom (6DOF) model, the constraint forces on the wires are calculated using the Udwadia-Kalaba equation and the external disturbances (atmospheric turbulence and gust) are included in the simulation. Simulation results are encouraging, thus making the proposed system an appealing candidate for similar applications.

Keywords: UAV, slung-load system, coordination control, obstacle avoidance, MPC.

1. Introduction

Recent developments in drone technology have made slung-load systems practical in both commercial and scientific applications [1, 2, 3]. In order to increase the maximum payload weight, a

[☆]This work is partly sponsored by the Research Council of Norway through the Centres of Excellence funding scheme, grant number 223254 – NTNU-AMOS

Email address: gaetano.tartaglione@uniparthenope.it (Gaetano Tartaglione)

slung-load system composed by a swarm of Unmanned Aerial Vehicles (UAVs) connected by wires to the payload is appealing.

There are two main challenges in the cooperative load transport problem. First of all, interactions among the UAVs, and between the UAVs and the payload are introduced by the wires. These interactions can be considered as external disturbances acting on the UAVs [1, 2]; then the control system must be designed including some requirements of robustness. Moreover, the control system must guarantee synchronization among the UAVs to obtain cooperation and to avoid collisions.

So far, to solve the cooperative load transport problem and its challenges, hierarchical controllers, geometrical controllers and nonlinear controllers have been used. We here explore the benefits of using Model Predictive Control (MPC) for designing a multi-level and distributed control system, computing the UAVs reference trajectories as the solution to a constrained optimization. The advantage of the proposed solution is the capability of taking into account dynamic operative scenarios, obstacle avoidance and performance constraints, control input saturation, requirement of robustness and sustainable computational cost.

1.1. Related works

Several works have focused on the control problem of cooperative load transport, proposing different approaches.

The geometrical controller introduced by T. Lee in [4] and [5] allows to follow a desired trajectory of both the payload position and attitude. In particular, the Voronoi tessellation technique is exploited to obtain the formation trajectory planning while taking into account collision-avoidance constraints. A geometrical controller is then designed using a coordinate-free form of the equations of motion, derived according to Lagrange mechanics.

Synchronization and tracking trajectory problems can be treated separately using a hierarchical controller. In [6] consensus and graph theory is employed for multi-copters synchronization and distributed control, respectively. In [7] first the controller computes the desired forces on the cables to follow the reference trajectory, then the reference position, speed and thrust of each UAV are computed to obtain the desired forces.

Other approaches are based on the use of nonlinear controllers, which enable to take into account the nonlinearity of the multi-copters dynamic model. In [8] a slung-load system composed of two quad-copters is modeled. The nonlinear controller is obtained by a partial feedback linearization

technique, and the collisions are avoided introducing a repulsion force among the UAVs. In [9] a nonlinear kinematic controller is used to compute the UAVs reference velocity vectors, through the feedback of the relative angles between the multi-copters and the load. In [10], the authors validate, by means of numerical simulations, a cooperative control strategy with coordination achieved through synchronization of the path parametrization, while the control law is computed using the back-stepping technique.

Experimental results are included in [11, 12], where the authors consider a swarm of indoor quad-copters to move the payload, and the control signals are obtained from the feedback of the UAVs and load positions provided by external cameras.

1.2. Contribution

In this paper, we propose a multi-level and distributed control system for a multi-body slung-load system. In particular, we consider different control modules to solve the following control problems: (i) trajectory planning; (ii) trajectory tracking; (iii) velocity and attitude control.

To obtain synchronization, the UAV reference trajectories are computed from the load trajectory assuming that the formation shape is known. The load trajectory is expressed as a sequence of way-points, which are the solution of a sequence of constrained optimization problems. This approach allows us to solve different coordination and cooperation problems [13], and it allows us to take into account operational constraints such as obstacles avoidance and UAV performance constraint. For this application, at each discrete time instant the new way-point is computed on the basis of the obstacle positions, the multi-copter cruise speed, the previous way-point and the target point.

The trajectory tracking module is based on a decentralized and robust MPC algorithm [14], in which at each discrete time instant each multi-copter solves only its own constrained optimization problem to obtain the control signals. This algorithm allows us to take into account the presence of control input saturations, the requirement of robustness and sustainable computational cost for a real application. The functional cost and the constraint functions are calculated assuming the knowledge of a reference trajectory and a prediction of the system behavior over a future horizon.

Finally, the control module for the control of UAV velocity and attitude is based on a PID control system, that computes the multi-copter motor speed on the basis of the MPC signal inputs.

We validate the designed flight control system by numerical simulations of a realistic scenario. In particular, the multi-copters are modeled as a rigid body and the 6DOF model [15] is used for the

simulation. The payload is modeled as a point mass in the space and the constraint forces on the wires acting on each drone are calculated using the Udwadia-Kalaba equation [16]. The controller robustness is tested by introducing atmospheric turbulence and gust in the simulations.

The paper is organized as follows. In Section 2 we describe the dynamic model of the multi-body system used for the numerical simulation. Section 3 presents the architecture of the flight control system. Section 4 illustrates the optimization problem for computing the load reference trajectory, while Section 5 illustrates the MPC optimization problem. In Section 6 we describe the scenarios which have been simulated and the numerical results; a comparison with some results appeared in [10] is also included. Finally, in Section 7 we draw some conclusions.

Notation. In the sequel by the symbol $\|\cdot\|$ we will denote the Euclidean norm, whereas by $\|\cdot\|_T$ we will denote the Euclidean norm weighted by the positive definite matrix T. By $A \succ 0$ we mean that each element of the matrix A is greater than 0. The symbol $\wedge$ denotes the cross product between two vectors. The symbol $\times$ denotes the Cartesian product between two sets. The symbols $\oplus$ and $\ominus$ denote respectively the Minkowski sum and the Pontryagin difference [17]. The symbol $(\cdot)^+$ denotes the Moore-Penrose Pseudo inverse [18]. With $\mathscr{C}^n(a)$ we denote the set obtained by $[-a;a]_1 \times [-a;a]_2 \times ...[-a;a]_n$, with I_n we denote the identity matrix of order n and with $0_{m\times n}$ we denote the $m-by-n$ matrix of zeros.

2. Slung-load system dynamic model

We consider a slung-load system composed by M identical multi-copters linked by M wires to a payload. In the following we describe the non linear dynamic model of each UAV, and the payload dynamics. Then we characterize the interconnected system by using the Udwadia-Kalaba equation, which allows us to compute constraint forces on the wires and acting on each UAV.

2.1. Multi-copter dynamic model

We introduce two reference frames: a body fixed frame B with origin O_B located in the Center of Gravity (CoG) of the UAV, and an inertial earth frame E. The dynamic equations in the inertial earth frame E are

$$\dot{V}_B = m^{-1}\left(-\Omega \wedge mV_B + \tau_g + \tau_p + \tau_w + \tau_a\right) \tag{1}$$

$$\dot{\Omega} = I_B^{-1}\left(-\Omega \wedge I_B\Omega + \nu_p + \nu_a\right) \tag{2}$$

where m and I_B are respectively the mass and inertial matrix of the multi-copter, V_B is the velocity vector in the body fixed frame and $\Omega = \begin{bmatrix}\Omega_x & \Omega_y & \Omega_z\end{bmatrix}^T$ is the angular velocity vector . In equations (1) and (2) external forces and moments need to be specified. More specifically, we consider the contributions of gravity force τ_g, the propulsive forces τ_p and moments ν_p, the aerodynamic drag τ_a and moments ν_a due to atmospheric turbulence and the constraint forces on the wire τ_w. Following the approach in [1] and in [16], we impose that the wires are connected from the CoG of the UAV to the CoG of the payload; under this assumption the UAVs attitude dynamics are unaffected.

The inertial position p is obtained from equations

$$\dot{p} = R_{BE}(\Theta)V_B \tag{3}$$

$$\dot{R}_{BE} = S(\Omega)R_{BE} \tag{4}$$

where $\dot{p} = \begin{bmatrix}V_x & V_y & V_z\end{bmatrix}^T$ is the velocity vector in the body inertial earth frame, Θ is the attitude with respect to the inertial earth frame, $R_{BE}(\Theta)$ is the rotation matrix from the body fixed frame to the inertial earth frame and $S(\Omega)$ is the skew-symmetric matrix operator defined as $S(\Omega) = \begin{bmatrix}0 & -\Omega_z & \Omega_y \\ \Omega_z & 0 & -\Omega_x \\ -\Omega_y & \Omega_x & 0\end{bmatrix}$.

2.2. Payload dynamic model

The payload is modeled as a point mass m_l in the space whose position p_l is obtained from

$$m_l\ddot{p}_l = [0 \quad 0 \quad m_l g]^T + \tau_l \tag{5}$$

where $\tau_l = -\sum_{i=1}^{M}\tau_w^{[i]}$ is the sum of the constraint forces on the wires connected to the UAVs.

2.3. Multi-body dynamic model

To find the interconnected system constraints we assume that the length d_{wire} of each wire is constant and the wires are taut. In particular, for the i-th wire we impose

$$\|L^{[i]}\|^2 - d_{wire}^2 = 0 \tag{6}$$

where $L^{[i]} = p^{[i]} - p_l$ is the vector between the i-th multi-copter and the payload. The constraint equation is obtained from the second derivative of equation (6)

$$2\ddot{L}^{[i]T} L^{[i]} + 2\dot{L}^{[i]T} \dot{L}^{[i]} = 0 \tag{7}$$

which, in order to use the Udwadia-Kalaba equation, may be rewritten in the following equivalent form:

$$A_{uk}^{[i]}(P,V)\dot{V} = b_{uk}^{[i]}(P,V)$$

where $P = [p^{[1]} \quad \dots \quad p^{[M]} \quad p_l]^T$, $V = [V_B^{[1]} \quad \dots \quad V_B^{[M]} \quad \dot{p}_l]^T$, $\tau_L = [\tau_w^{[1]} \quad \dots \quad \tau_w^{[M]} \quad \tau_l]^T$. More specifically

$$A_{uk}^{[i]} = L^{[i]T} \begin{bmatrix} 0_{3\times 3(i-1)} & R_{BE}^{[i]} & 0_{3\times 3(M-1)} & -I_3 \end{bmatrix}$$

$$b_{uk}^{[i]} = -L^{[i]T} S(\Omega^{[i]}) R_{BE}^{[i]} V_B^{[i]} - \dot{L}^{[i]T} \dot{L}^{[i]}$$

and according to [16] the vector τ_L is computed though the Udwadia-Kalaba equation

$$\tau_L = M^{\frac{1}{2}} (A_{uk} M^{-\frac{1}{2}})^{+} (b_{uk} - A_{uk}\dot{v}) \tag{8}$$

where M, A_{uk}, b_{uk} are the concatenations of $m^{[i]}$, $A_{uk}^{[i]}$, $b_{uk}^{[i]}$ and $\dot{v}$ collects the UAVs and payload unconstrained accelerations. Equation (8) is used to develop the multi-body slung-load simulator.

3. Control system architecture

The control system is made of two main parts as shown in Figure 1: the reference trajectory layer and the multi-copter flight control system.

The reference trajectory layer is implemented in a central unit, e.g. the control ground station, and it is characterized by the sampling time Δt. The multi-copter flight-control system is

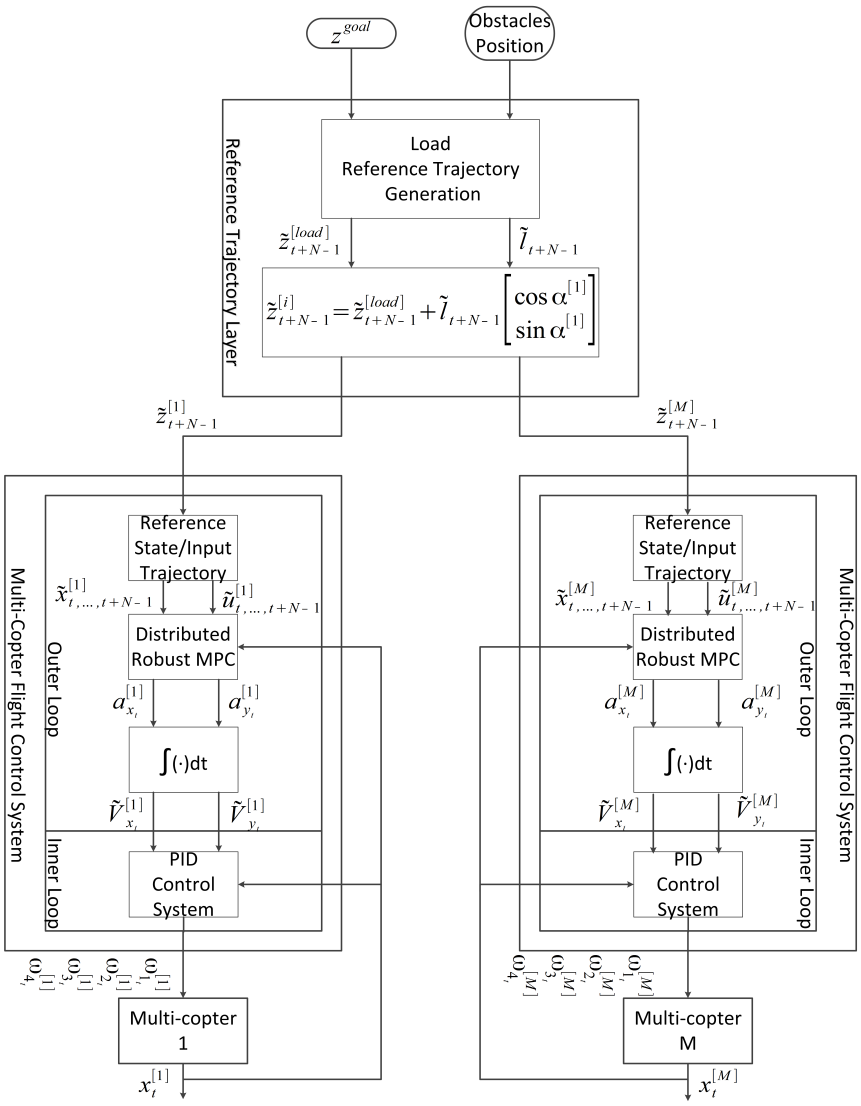

Figure 1: Slung-Load Control System Architecture

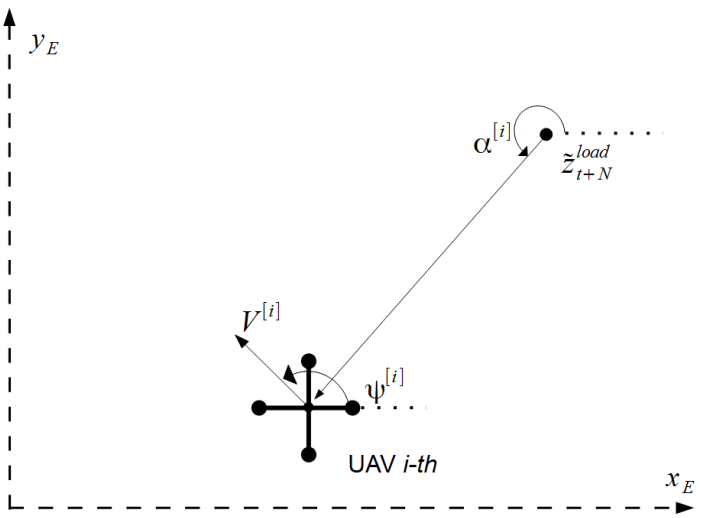

Figure 2: Shape Formation Definition

implemented on board and is characterized by two control loops with two different sampling times, denoted by Δt and Δt_{inner} for the outer and inner loops, respectively, with $\Delta t > \Delta t_{inner}$. We assume that the control ground station and the UAVs flight-control systems are linked through an ideal (instantaneous and error-free) communication network.

The inputs of the reference trajectory layer are the final payload position z^{goal} and the position of the no-fly zones, while the outputs are the reference trajectory of each multi-copter defined as a sequence of way-points. In particular, at the discrete time instant t the reference trajectory layer computes the UAVs way-points at discrete time instant $t+N-1$, where N is the length of the optimization horizon of the MPC technique. Assuming mission at constant and fixed altitude, the way-point of the i-th multi-copter $\tilde{z}^{[i]}_{t+N-1}$ at the time instant $t+N-1$ is obtained by the knowledge of the projection of the payload trajectory in the UAVs horizontal plane, on the basis of the distance $\tilde{l}_{t+N-1}$ and the angle $\alpha^{[i]}$ (see Figure 2)

$$\tilde{z}^{[i]}_{t+N-1} = \tilde{z}^{[load]}_{t+N-1} + \tilde{l}_{t+N-1} \begin{bmatrix} \cos\alpha^{[i]} \\ \sin\alpha^{[i]} \end{bmatrix} \tag{9}$$

where $\alpha^{[i]}$ is a fixed geometric configuration parameter of the slung-load system, while the point

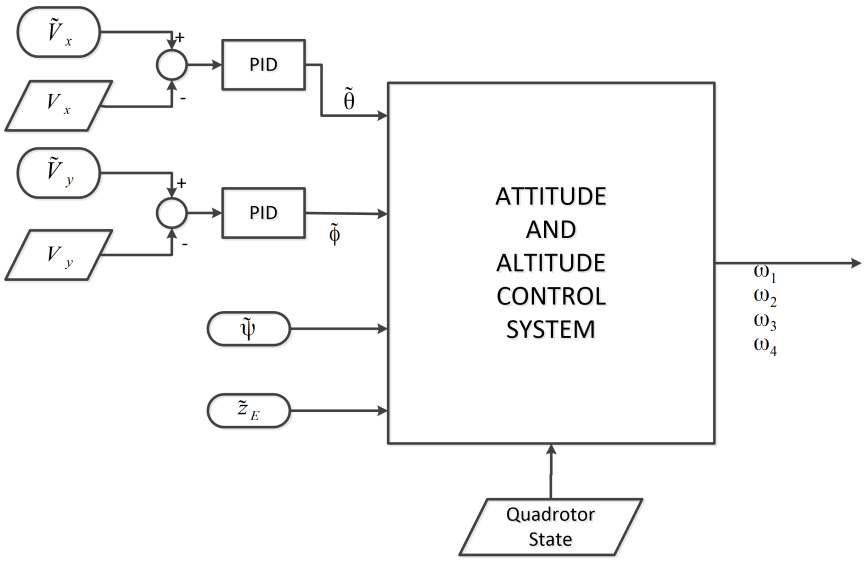

Figure 3: Inner Loop Architecture

$\tilde{z}^{[load]}_{t+N-1}$ and the distance $\tilde{l}_{t+N-1}$ are computed at each discrete time instant by the reference trajectory layer as the solution of the constrained optimization problem described in the following section.

Considering the flight control system of the i-th multi-copter, the outer loop implements a robust MPC algorithm to compute the reference inertial velocities $\tilde{V}^{[i]}_{x_t}$ and $\tilde{V}^{[i]}_{y_t}$ that are the input to the inner loop. To define the MPC optimization problem, we need to compute the sequences of reference states $\tilde{x}^{[i]}_{\{t,\ldots,t+N-1\}}$ and input $\tilde{u}^{[i]}_{\{t,\ldots,t+N-1\}}$ from the sequence of way-points of the reference trajectory, and for this reason we introduce in the outer loop the reference state/input trajectory layer. The reference velocity is finally obtained from the MPC control input $a^{[i]}_{x_t}$ and $a^{[i]}_{y_t}$.

The inner loop computes the multi-copter motors speed by means of two PID control systems to obtain pitch $\tilde{\theta}$ and roll $\tilde{\phi}$ references angles (Figure 3):

$$\tilde{\theta}(t) = K_p e_x(t) + K_i \int_0^t e_x(\tau)d\tau + K_d \frac{de_x(t)}{dt}$$
$$\tilde{\phi}(t) = K_p e_y(t) + K_i \int_0^t e_y(\tau)d\tau + K_d \frac{de_y(t)}{dt}$$

where $e_x(t) = \tilde{V}_x - V_x$, $e_y(t) = \tilde{V}_y - V_y$ are the difference between the UAV inertial velocities and the reference velocities and K_p, K_i, K_d are the control gains. Finally, for the attitude and altitude

control, we use the classical approach described in [19].

4. Reference Trajectory Generation

At each discrete time instant t, the reference trajectory layer sends to each flight-control system the corresponding UAV reference trajectory over a future horizon of length N using a receding horizon strategy, where only the new way-point at time $t+N-1$ is calculated.

Basing on equation (9), the UAV reference trajectories are computed from the load position $\tilde{z}^{[load]}_{t+N-1}$ and distance $\tilde{l}_{t+N-1}$. To obtain feasible trajectories, operational constraints about the multi-copter positions are taken into account. In particular, the points $\tilde{z}^{[i]}_{t+N-1}$ for $i = 1, \ldots, M$ can be obtained from the optimization parameters as

$$\tilde{z}^{[i]}_{t+N-1} = \begin{bmatrix} 1 & 0 & \cos\alpha^{[i]} \\ 0 & 1 & \sin\alpha^{[i]} \end{bmatrix} \begin{bmatrix} \tilde{z}^{[load]}_{t+N-1} \\ \tilde{l}_{t+N} \end{bmatrix} \tag{10}$$

Then, the reference trajectory layer at each discrete time instant computes the solution of the following constrained optimization problem

$$\min_{\tilde{z}^{[load]}_{t+N-1}, \tilde{l}_{t+N-1}} \beta\Big(\gamma \left\| \tilde{z}^{[load]}_{t+N-1} - \tilde{z}^{[load]}_{t+N-2} \right\|^2 + \left\| \tilde{z}^{[load]}_{t+N-1} - z^{goal} \right\|^2_T\Big) + (1-\beta) \left\| \tilde{l}_{t+N-1} - \bar{l} \right\|^2 \tag{11}$$

subject to obstacle avoidance constraints and

$$\tilde{z}^{[load]}_{t+N-1} \in \mathscr{B}_{t+N-1} \tag{12a}$$

$$\tilde{z}^{[i]}_{t+N-1} \in \mathbb{Z} \quad i = 1, ..., M \tag{12b}$$

$$\tilde{l}_{t+N-1} \in [\underline{l}; \bar{l}] \tag{12c}$$

The quadratic cost function (11) is the linear combination of two terms: the former related to the distance from the target and the latter related to the formation shape. More specifically, the first term allows us to minimize the payload distance from the target, while the second one allows us to maximize the plan distance between the payload and the multi-copters, and consequently the distances between the multi-copters. The cost function is calculated from the trajectory point $\tilde{z}^{[load]}_{t+N-2}$, the final trajectory point $\tilde{z}^{goal}$ and the reference load-UAV distance $\bar{l}$. The weights T, γ and β are tuning knobs satisfying $T \succ \gamma I_2 \succ 0$ and $0 < \beta < 1$. In particular, when $\beta \to 0$ the

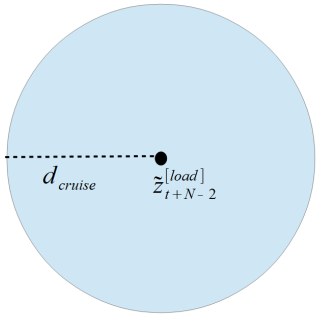

Figure 4: Set $\mathscr{B}_{t+N-1}$

distances between the UAVs are constant, while with $\beta \to 1$ we relax the constraint on the distances between the UAVs, and in this case the payload reference trajectory will be closer to the obstacles.

The constraint (12a) allows us to control the norm of the payload inertial velocity. In particular, the set $\mathscr{B}_{t+N-1}$ is a circular set of center $\tilde{z}^{[load]}_{t+N-2}$ and radius $d_{cruise} = \Delta t V_{cruise}$ (see Figure 4), where V_{cruise} is the reference for the norm of the payload inertial speed.

The constraint (12b) guarantees that the reference states $\tilde{x}^{[i]}_{\{t,\dots,t+N-1\}}$ computed from the sequence of way-points of the reference trajectory, to define the MPC problem, are feasible. The set $\mathbb{Z}$ depends on the algorithm applied in the outer control loop. For this reason, the set $\mathbb{Z}$ is computed after defining MPC optimization problem using the algorithm in [13].

The constraint (12c) avoids collisions among the UAVs and guarantees distances shorter than wires length. Then, $\underline{l}$ and $\bar{l}$ are fixed satisfying

$$\underline{l} > \frac{d_{UAV} + \delta}{\sin \frac{\pi}{M}} \tag{13a}$$

$$\bar{l} < d_{wire} \tag{13b}$$

Obstacle avoidance constraints are formulated by ensuring coordination between multi-copters. Then, the new way-points allow all multi-copters to avoid the no-fly zone without breaking up the formation. Referring to the i-th multi-copter and the h-th obstacle, if the obstacle is circular with

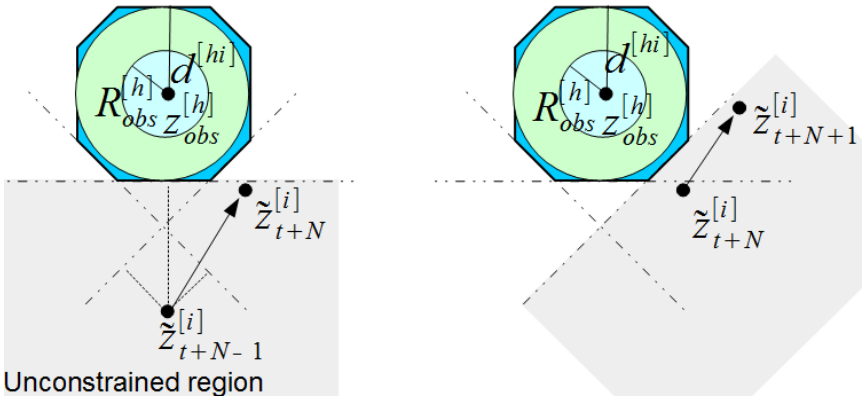

Figure 5: Linear approximation for obstacle avoidance constraints

center in $z^{[h]}_{obs}$ and radius $R^{[h]}_{obs}$, the obstacle avoidance constraint can be formulated as

$$\left\| \tilde{z}^{[i]}_{t+N-1} - z^{[h]}_{obs} \right\| \geq d^{[hi]} \tag{14}$$

where $d^{[hi]} = R^{[h]}_{obs} + d_{UAV} + \delta$, d_{UAV} is the radius of the circle surrounding the multi-copters and the distance δ is a safety distance which takes into account the maximum uncertainty about the UAV positions. This distance is estimated using the algorithm in [13]. Moreover, to avoid collision between wires and obstacles, we impose $d^{[hi]} > \bar{l}/2$. If the h-th obstacle is not circular, we introduce a circular no-fly zone that surrounds the obstacle so to follow the same approach described above. In order to deal with the nonlinearity and the non-convexity of the constraint in (14), we apply a linear approximation as described in [13]. We build a polytope $\mathscr{P}^{[hi]}_{obs}$ with $r^{[hi]}_{obs}$ edges that circumscribes the no-fly zone centered in $z^{[h]}_{obs}$ with radius $d^{[hi]}$ and we introduce the linear operator $\rho^{[hi]}(k)$ which computes the distance between the trajectory point of i-th multi-copter and the k-th edge of the polytope $\mathscr{P}^{[hi]}_{obs}$ (as shown in Figure 5)

$$\rho^{[hi]}(k) = \frac{1}{\sqrt{{a^{[hi]}_k}^2 + {b^{[hi]}_k}^2}} \begin{bmatrix} a^{[hi]}_k & b^{[hi]}_k & 1 \end{bmatrix} \begin{bmatrix} \tilde{z}^{[i]}_{t+N-1} \\ 1 \end{bmatrix} \tag{15}$$

where $a^{[hi]}_k$ and $b^{[hi]}_k$ are the coefficients that define the equation of the k-th edge of the polytope $\mathscr{P}^{[hi]}_{obs}$. It is worth noting that this *linearization* of the constraint (14) is conservative only because the circular no-fly zone is approximated by means of a polytope.

5. Model Predictive Control Algorithm

The control inputs to track the reference trajectory are calculated by implementing a distributed and robust MPC algorithm. Each UAV computes its own control inputs independently from the other multi-copters using the same algorithm. Indeed the interaction between the aircrafts has already been taken into account by the reference trajectory layer.

To implement the robust MPC algorithm, the outer control loop solves a constrained optimization problem at each discrete time instant. The cost and constraint functions are evaluated by using the reference trajectory and a prediction of the UAV behavior. For this application, to predict the multi-copter behavior we use the dynamic model of a material point in the plane. The sequences of reference states and inputs are calculated from the geometrical reference trajectory by the input/state layer (see Figure 1).

5.1. Definition of the nominal model

The dynamic model of a material point in the plane can be defined in terms of position in the inertial earth frame $\begin{bmatrix} x_E & y_E \end{bmatrix}$, course angle Ψ and linear speed V:

$$\begin{cases} \dot{x}_E = V \cos \Psi \\ \dot{y}_E = V \sin \Psi \\ \dot{\Psi} = \omega \\ \dot{V} = a \end{cases} \tag{16}$$

where the input of system are the angular velocity ω and the linear acceleration a.

We obtain a linear model of a material point (16) following the procedure described in [20]. Letting $\eta_1 = x_E$, $\eta_2 = \dot{x}_E$, $\eta_3 = y_E$, $\eta_4 = \dot{y}_E$ and introducing the linear accelerations a_x and a_y, we obtain a set of two decoupled double integrators

$$\begin{cases} \dot{\eta}_1 = \eta_2 \\ \dot{\eta}_2 = a \cos \Psi - V \omega \sin \Psi \equiv a_x \\ \dot{\eta}_3 = \eta_4 \\ \dot{\eta}_4 = a \sin \Psi + V \omega \cos \Psi \equiv a_y \end{cases} \tag{17}$$

We compute a discretization of equation (17) with sampling time Δt by means of the following Euler discretization:

$$x_{t+1} = Ax_t + Bu_t + w_t \tag{18a}$$

$$z_{t+1} = Cx_{t+1} \tag{18b}$$

where

$$x_t = \begin{bmatrix} \eta_{1_t} & \eta_{2_t} & \eta_{3_t} & \eta_{4_t} \end{bmatrix}^T, \quad u_t = \begin{bmatrix} a_{x_t} \\ a_{y_t} \end{bmatrix}, z_t = \begin{bmatrix} x_{E_t} \\ y_{E_t} \end{bmatrix},$$

$$A = \begin{bmatrix} 1 & \Delta t & 0 & 0 \\ 0 & 1 & 0 & 0 \\ 0 & 0 & 1 & \Delta t \\ 0 & 0 & 0 & 1 \end{bmatrix}, \quad B = \begin{bmatrix} \frac{\Delta t^2}{2} & 0 \\ \tau & 0 \\ 0 & \frac{\Delta t^2}{2} \\ 0 & \tau \end{bmatrix}, \quad C = \begin{bmatrix} 1 & 0 & 0 & 0 \\ 0 & 0 & 1 & 0 \end{bmatrix}.$$

The disturbance w_t has been introduced to model uncertainties and approximation errors of the UAV model and external disturbances due to the atmospheric turbulence and the constraint forces on wires, which are included in the simulator using the Udwadia-Kalaba equation (8) but considered unknown in the control design. We assume that $w_t \in \mathbb{W}$, where $\mathbb{W}$ is a known bounded uncertainty set. We denote the set of feasible states by $x_t \in \mathbb{X}$, where $\mathbb{X}$ is a convex set. It can be readily verified that the triple (A, B, C) is reachable, observable, and does not have invariant zeros on the unit circle.

5.2. Reference state/input trajectory

In order to calculate the cost function of the optimization problem, the sequence of references states $\tilde{x}^{[i]}_{\{t,\dots,t+N-1\}}$ and inputs $\tilde{u}^{[i]}_{\{t,\dots,t+N-1\}}$ of the nominal model must be computed from the sequence of N geometrical points $\tilde{z}^{[i]}_{\{t,\dots,t+N-1\}}$.

To solve this problem, we implement in the state/input trajectory layer the following dynamic system

$$\begin{bmatrix} \tilde{x}^{[i]}_{t+1} \\ \tilde{e}^{[i]}_{t+1} \end{bmatrix} = \begin{bmatrix} A & 0 \\ -C & I_2 \end{bmatrix} \begin{bmatrix} \tilde{x}^{[i]}_{t} \\ \tilde{e}^{[i]}_{t} \end{bmatrix} + \begin{bmatrix} B \\ 0 \end{bmatrix} \tilde{u}^{[i]}_t + \begin{bmatrix} 0 \\ I_2 \end{bmatrix} \tilde{z}^{[i]}_{t+1} \tag{19}$$

where the new state variable $\tilde{e}^{[i]}_{t+1}$ is the integral of the tracking error $\tilde{z}^{[i]}_{t+1} - C\tilde{x}^{[i]}_t$. Given the reachability of the pair (A, B) and the absence of invariant zeros in $z = 1$ of the model (18a), it is

possible to compute the control law

$$\tilde{u}_t^{[i]} = \tilde{K}_x \tilde{x}_t^{[i]} + \tilde{K}_e \tilde{e}_t^{[i]} \tag{20}$$

where the gain $\tilde{K} = \begin{bmatrix} \tilde{K}_x & \tilde{K}_e \end{bmatrix}$ can be designed with any stabilizing algorithm, such as LQ or pole placement control.

5.3. Definition of the MPC optimization problem

At each discrete time instant the i-th flight control system solves the following constrained optimization problem in order to implement the robust MPC algorithm discussed in [14]

$$\min_{\hat{x}_t^{[i]}, \hat{u}_{\{t,\dots,t+N-1\}}^{[i]}} \sum_{j=0}^{N-1} \left\| \hat{x}_{t+j}^{[i]} - \tilde{x}_{t+j}^{[i]} \right\|_Q^2 + \left\| \hat{u}_{t+j}^{[i]} - \tilde{u}_{t+j}^{[i]} \right\|_R^2 + \left\| \hat{x}_{t+N}^{[i]} - \tilde{x}_{t+N}^{[i]} \right\|_P^2 \tag{21}$$

subject to

$$\hat{x}_{t+1}^{[i]} = A\hat{x}_t^{[i]} + B\hat{u}_t^{[i]} \tag{22a}$$

$$\hat{x}_{t+j}^{[i]} \in \hat{\mathbb{X}}^{[i]}, \quad \forall j = 1, ..., N-2 \tag{22b}$$

$$x_t^{[i]} - \hat{x}_t^{[i]} \in \varepsilon^{[i]} \tag{22c}$$

$$C(\hat{x}_{t+j}^{[i]} - \tilde{x}_{t+j}^{[i]}) \in \Delta_z^{[i]}, \forall j = 1, ..., N-2 \tag{22d}$$

$$x_{t+N-1}^{[i]} - \hat{x}_{t+N-1}^{[i]} \in \kappa^{[i]} \varepsilon^{[i]} \tag{22e}$$

The set $\varepsilon^{[i]}$ in (22c) is defined as the robust positively invariant (RPI) set

$$\varepsilon^{[i]} = \bigoplus_{j=0}^{\infty} (A + BK)^j \mathbb{W}^{[i]} \tag{23}$$

where the gain K must be defined so as to obtain $(A + BK)$ to be Schur stable. In particular, we compute $\varepsilon^{[i]}$ as an outer approximation of the minimum RPI using the method discussed in [21]. The set $\hat{\mathbb{X}}^{[i]}$ in (22b) is computed as

$$\hat{\mathbb{X}}^{[i]} = \mathbb{X}^{[i]} \ominus \varepsilon^{[i]} \tag{24}$$

The set $\Delta_z^{[i]} \subseteq \mathbb{R}^2$ in (22d) is characterized by a trade-off: a small size of this set permits

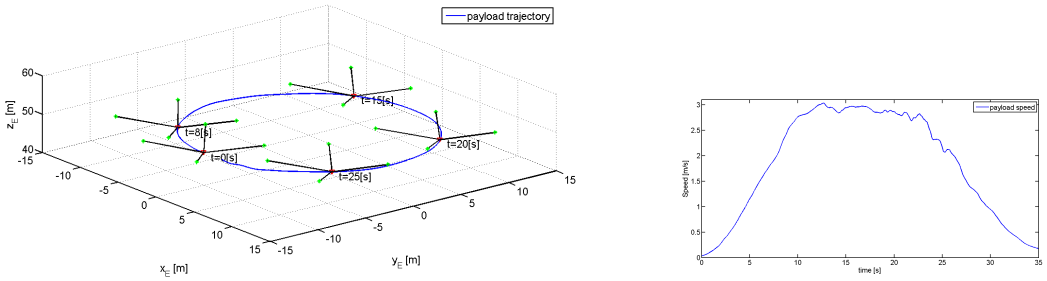

(a) *Snapshots of payload trajectory at different times.* (b) *Payload speed.*

Figure 6: Scenario simulated to test the performance of the trajectory tracking and speed and attitude control modules. This scenario is taken from[10]

only small deviations of the nominal state trajectory with respect to the reference, but it can have the effect of limiting the robustness of the control scheme. Finally, $\kappa^{[i]} > 0$ in (22e) is a tuning parameter.

In the functional cost, the symmetric weighting matrices $Q \geq 0$ and $R > 0$ are free design parameters, while P is assumed to satisfy the Lyapunov equation

$$(A + BK)^T P(A + BK) - P = -(Q + K^T RK) \tag{25}$$

From the solution of the optimization problem we obtain $\hat{u}^{[i]}_{t|t}$ and $\hat{x}^{[i]}_t$, and the control inputs for the i-th multi-copter are calculated as

$$u^{[i]}_t = \hat{u}^{[i]}_{t|t} + K(x^{[i]}_t - \hat{x}^{[i]}_t) \tag{26}$$

6. Numerical Simulations

The proposed flight control system was tested using *Simulink*. We developed a simulator of a multi-body slung-load system composed by $M = 4$ *micro* quad-copters with $m = 1.4kg$, $d_{UAV} = 0.3m$ and $\alpha^{[i]} = i\pi/2$ for $i = 1, .., 4$, the payload was assumed to have mass $m_l = 0.4kg$.

As a first example, we have considered the scenario simulated in [10], where the authors use a nonlinear controller based on back-stepping technique. In this case, the trajectory is assigned, both in terms of position and velocity, and hence we test only our modules for trajectory tracking and velocity and attitude control. In particular, the payload is moved along a circular path of radius

$R = 10m$, accelerating to a maximum speed of $3m/s$, and then slowed down to zero. Figures 6 show the performance obtained with our MPC, which are comparable with those presented in [10].

Then we have considered an example to test all the features of our control system. To this aim we have considered a scenario in which the payload has to be moved from the point $\begin{bmatrix}5.0 & 5.0\end{bmatrix} m$ to the point $\begin{bmatrix}100.0 & 100.0\end{bmatrix} m$ in a region characterized by four circular obstacles with:

$$
\begin{aligned}
z_{obs}^{[1]} &= \begin{bmatrix}40.0 & 45.5\end{bmatrix} m, \quad R_{obs}^{[1]} = 5.0m \\
z_{obs}^{[2]} &= \begin{bmatrix}40.0 & 24.5\end{bmatrix} m, \quad R_{obs}^{[2]} = 5.0m \\
z_{obs}^{[3]} &= \begin{bmatrix}70.0 & 57.0\end{bmatrix} m, \quad R_{obs}^{[3]} = 5.0m \\
z_{obs}^{[4]} &= \begin{bmatrix}70.0 & 70.0\end{bmatrix} m, \quad R_{obs}^{[4]} = 5.0m
\end{aligned}
$$

In order to allow a real-time implementation we have chosen $\Delta t = 0.5s$ and $\Delta t_{inner} = 0.01s$.

The free-tuning parameters of the flight control system has been fixed through a trial and error procedure to obtain satisfying performance in the absence of atmospheric disturbances. In particular, the MPC optimization problem (22) has been defined by setting the following parameters. Considering the mission goal and the UAV performance we have set $\mathbb{X}^{[i]} = \begin{bmatrix}0.0 & 110.0\end{bmatrix} \times \begin{bmatrix}-5.0 & 5.0\end{bmatrix} \times \begin{bmatrix}0.0 & 110.0\end{bmatrix} \times \begin{bmatrix}-5.0 & 5.0\end{bmatrix}$ for $i = 1, \ldots, 4$ (dimension in m and m/s, respectively). For each $i = 1, \ldots, 4$, we have set $\mathbb{W}^{[i]} = \mathscr{C}^4(0.01)$, $\Delta_z^{[i]} = \mathscr{C}^2(0.001)$ and $\kappa^{[i]} = 10^5$. The cost function has been defined by the length of the prediction horizon $N = 10$ and the weighting matrices $Q = I_4$ and $R = 180I_2$. Finally, the matrix K is the gain of the LQ regulator with the weighting matrices Q and R. The matrix $\tilde{K}$ used to compute the reference control law (20) is the gain of the LQ regulator with the weighting matrices $\tilde{Q} = I_6$ and $\tilde{R} = 2000I_2$. To compute the reference trajectory, the optimization problem (12) has been defined setting $\gamma = 1$, $T = 10I_2$, $\underline{l} = 3$ and $\bar{l} = 5$. The coefficient β has been fixed by analyzing the different reference trajectories, i.e. in Figure 7 we show the two trajectories obtained setting respectively $\beta = 10^{-3}$ and $\beta = 10^{-5}$. In particular, we have chosen $\beta = 10^{-3}$ to relax the constraint on the distances between the UAVs and the payload, and in this way the payload reference trajectory passes through the obstacles #1 and #2 avoiding quick changes of direction.

The flight control system robustness has been tested by simulating the above scenario with different atmospheric disturbances. We have considered the Von Karman wind turbulence model

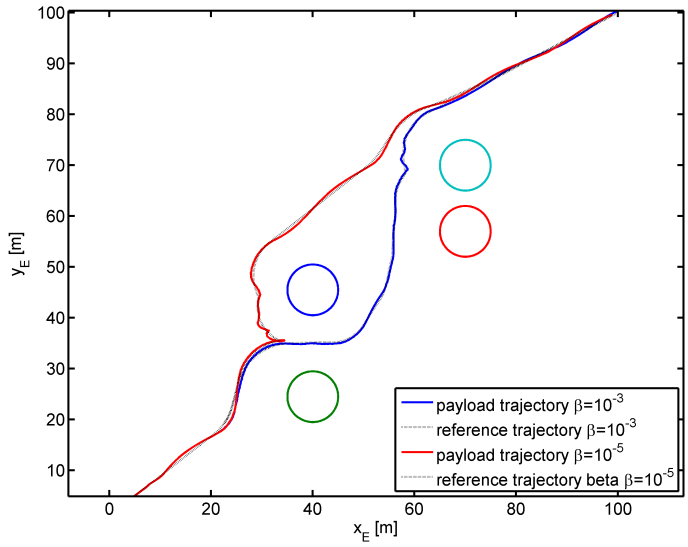

Figure 7: Payload trajectories at different β values

and the discrete wind gust model by using the *Simulink Aerospace Blockset*, according to the references [22, 23]. We have defined twenty five realistic atmospheric conditions by setting five amplitude values for gust model and five wind speed values for turbulence model and we have analyzed the performance decay, the growing of the constraints forces and the fulfillment of collision avoidance constraints. The performance of the slung-load control system have been evaluated through the tracking trajectory error

$$E(i) = \left\| z^{[l]}_{t_0+i\Delta t} - \tilde{z}^{[l]}_{t_0+i\Delta t} \right\| \tag{27}$$

More specifically, we have considered the mean of the tracking trajectory error

$$E_{mean} = \frac{1}{N_{tot}} \sum_{i=0}^{N_{tot}} E(i) \tag{28}$$

and the maximum of the tracking trajectory error

$$E_{max} = \max\{E(1), E(2), ..., E(N_{tot})\} \tag{29}$$

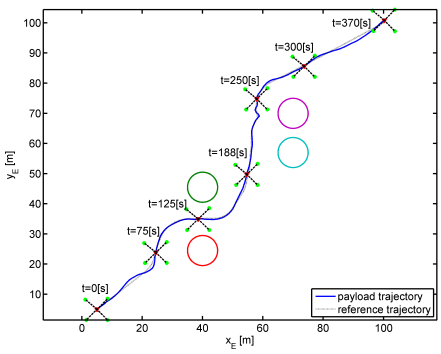

(a) *Payload trajectory in inertial frame.*

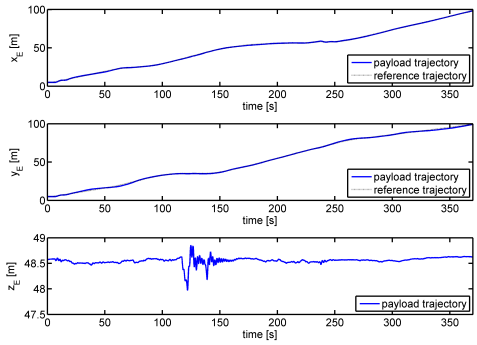

(b) *Actual trajectories.*

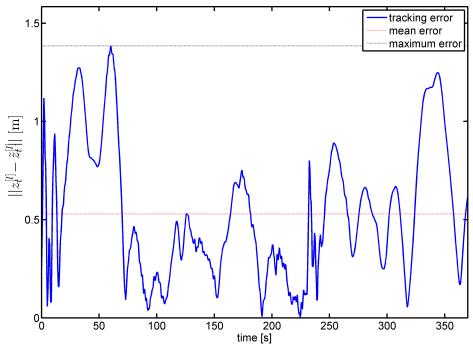

(c) *Payload tracking error.*

Figure 8: Trajectory tracking performance

as performance indexes.

As an example of the results obtained, in the following we show the results for the simulation characterized by amplitude gust $V_{gust} = \begin{bmatrix} 2 & 2 & 0 \end{bmatrix}^T m/s$ and turbulence wind speed $V_{turb} = 5m/s$.

Figures 8a and 8b show a comparison between the payload reference trajectory and the actual trajectory. The tracking error is shown in Figure 8c and the performance indexes are $E_{mean} = 0.53m$ and $E_{max} = 1.38m$.

In spite of the tracking error, the collision and obstacle avoidance constraints are satisfied. Figures 9 show that the no-fly zones are not violated and the minimum safety distances between UAV 1 and others are satisfied.

To evaluate the feasibility of the slung-load control system, we have checked the constraint

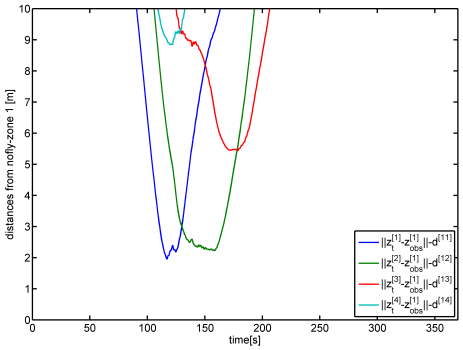

(a) *Distances from no-fly zone 1.*

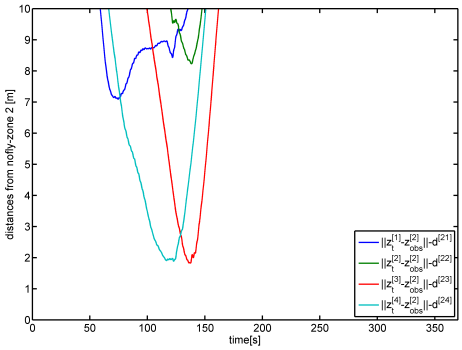

(b) *Distances from no-fly zone 2.*

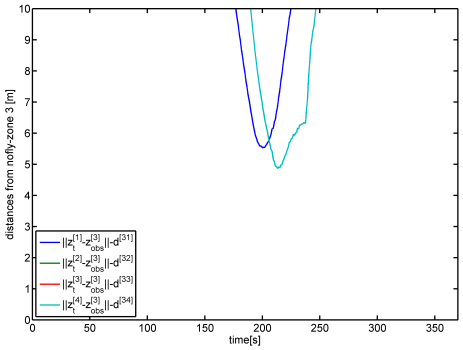

(c) *Distances from no-fly zone 3.*

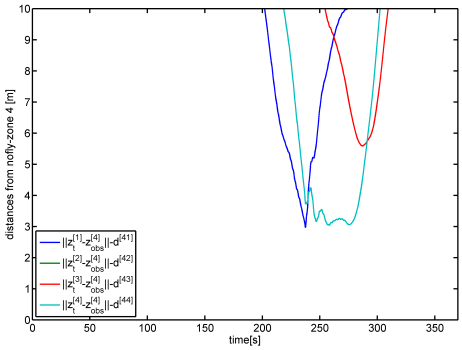

(d) *Distances from no-fly zone 4.*

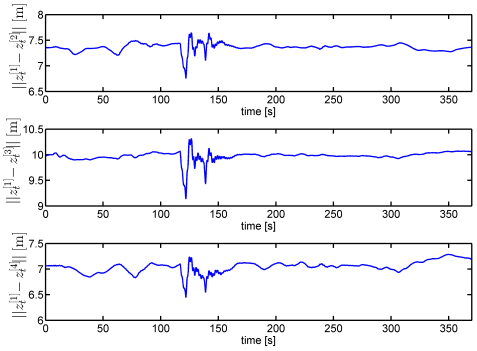

(e) *Distances from UAV #1.*

Figure 9: Collision and obstacles constraints time evolution

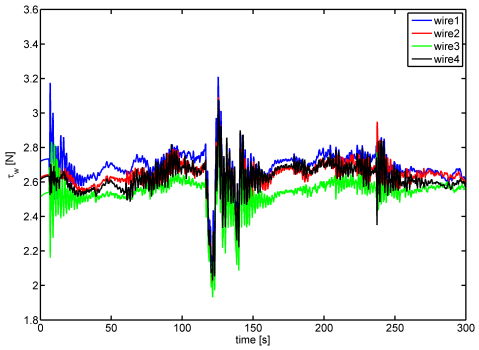

(a) *Constraint forces.*

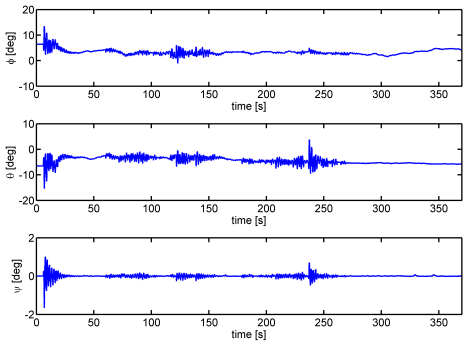

(b) *UAV 1 attitude.*

Figure 10: Constraint and attitude plot

force magnitudes to avoid wires breaking, and we have checked the quad-copters attitude to avoid unrealistic maneuvers. Figure 10a shows that the greatest forces are obtained during the initial acceleration and maneuvers to change the planar distance between payload and quad-copters. Figure 10b shows the attitude of quad-copter #1 during the flight mission: it can be seen that the flight control system has required realistic maneuvers.

The performance of the flight control system when the atmospheric conditions vary, are synthesized in Table 1. In particular, as expected, the performance worsen when increasing the disturbances, but the mission goal is completed and the collisions are avoided with realistic maneuvers and constraint forces in all cases except the most severe conditions.

With the most severe atmospheric conditions, the slung-load control system is not able to complete the flight mission. To complete the mission in this condition, we needed to change the set of parameters of the flight control system. In particular, we have increased the uncertainty set, i.e. fixing $\mathbb{W}^{[i]} = \mathscr{C}^4(0.02)$ for each $i = 1, ..., 4$, to consider the external disturbances due to atmospheric conditions. In this way, the slung-load control system is able to complete the mission with the performance indexes shown in Table 2.

7. Conclusions

In this paper, a multi-level and distributed control system for a multi-body slung-load system based on MPC has been proposed. The control system is composed by different control modules

	$V_{gust} = \begin{bmatrix}1\\1\\0\end{bmatrix}$	$V_{gust} = \begin{bmatrix}1.5\\1.5\\0\end{bmatrix}$	$V_{gust} = \begin{bmatrix}2\\2\\0\end{bmatrix}$	$V_{gust} = \begin{bmatrix}2.5\\2.5\\0\end{bmatrix}$	$V_{gust} = \begin{bmatrix}3\\3\\0\end{bmatrix}$
$V_{turb} = 0$	$E_{mean} = 0.35$ $E_{max} = 1.12$	$E_{mean} = 0.36$ $E_{max} = 1.12$	$E_{mean} = 0.37$ $E_{max} = 1.12$	$E_{mean} = 0.39$ $E_{max} = 1.12$	$E_{mean} = 0.38$ $E_{max} = 1.24$
$V_{turb} = 2.5$	$E_{mean} = 0.40$ $E_{max} = 1.12$	$E_{mean} = 0.43$ $E_{max} = 1.12$	$E_{mean} = 0.46$ $E_{max} = 1.15$	$E_{mean} = 0.50$ $E_{max} = 1.31$	$E_{mean} = 0.52$ $E_{max} = 1.38$
$V_{turb} = 5$	$E_{mean} = 0.45$ $E_{max} = 1.17$	$E_{mean} = 0.48$ $E_{max} = 1.26$	$E_{mean} = 0.53$ $E_{max} = 1.38$	$E_{mean} = 0.60$ $E_{max} = 1.56$	$E_{mean} = 0.67$ $E_{max} = 2.15$
$V_{turb} = 7.5$	$E_{mean} = 0.49$ $E_{max} = 1.29$	$E_{mean} = 0.57$ $E_{max} = 1.60$	$E_{mean} = 0.67$ $E_{max} = 1.92$	$E_{mean} = 0.72$ $E_{max} = 2.15$	mission not completed
$V_{turb} = 10$	$E_{mean} = 0.60$ $E_{max} = 1.89$	$E_{mean} = 0.69$ $E_{max} = 1.99$	$E_{mean} = 0.73$ $E_{max} = 2.04$	mission not completed	mission not completed

Table 1: Performance indexes in different atmospheric conditions

	$V_{gust} = \begin{bmatrix}2.5\\2.5\\0\end{bmatrix}$	$V_{gust} = \begin{bmatrix}3\\3\\0\end{bmatrix}$
$V_{turb} = 7.5$	. .	$E_{mean} = 1.47$ $E_{max} = 4.80$
$V_{turb} = 10$	$E_{mean} = 1.37$ $E_{max} = 5.72$	$E_{mean} = 1.72$ $E_{max} = 6.86$

Table 2: Performance indexes in the worst atmospheric conditions

to solve trajectory planning, trajectory tracking and velocity and attitude control, while taking into account multi-copter performance constraints, obstacle avoidance constraints, the presence of input saturations, robustness requirements and computational cost. The first step of the algorithm consists of the calculation of the reference trajectory of each UAV as solution of a constrained optimization problem, then optimal guidance laws are calculated based on a MPC algorithm, finally PID control systems allow to control of the UAV speed and attitude. A simulator has been developed and different atmospheric disturbances has been considered to test the proposed control system and its robustness. The numerical results show the effectiveness of the proposed approach. Further work will consist in implementing the control algorithm in a real-time application to carry out flight tests.

References

[1] M. Bisgaard, Modeling, estimation, and control of helicopter slung load system, Ph.D. thesis, Aalborg Universitet (2008).

[2] I. Palunko, P. Cruz, R. Fierro, Agile load transportation : Safe and efficient load manipulation with aerial robots, IEEE Robotics & Automation Magazine 19 Issue 3 (2012) 69–79.

[3] K. Klausen, T. Fossen, T. Johansen, Nonlinear control of a multirotor UAV with suspended load, in: IEEE International Conference on Unmanned Aircraft Systems, 2015, pp. 176–184.

[4] T. Lee, Geometric control of multiple quadrotor UAVs transporting a cable-suspended rigid body, in: IEEE Conference on Decision and Control, 2014.

[5] T. Lee, Collision avoidance for quadrotor UAVs transporting a payload via voronoi tessellation, in: IEEE American Control Conference, 2015.

[6] W. Ren, R. Beard, E. Atkins, A survey of consensus problems in multi-agent coordination, in: IEEE American Control Conference, 2005, pp. 1859–1864 vol 3.

[7] Z. Li, J. Horny, J. Langelaanz, Coordinated transport of a slung load by a team of autonomous rotorcraft, in: AIAA Guidance, Navigation, and Control Conference, 2014.

[8] I. Pizetta, A. Brandao, M. Sarcinelli-Filho, Cooperative quadrotors carrying a suspended load, in: IEEE International Conference on Unmanned Aircraft Systems, 2016.

[9] K. Klausen, T. Fossen, T. Johansen, Suspended load motion control using multicopters, in: IEEE Mediterranean Conference of Control and Automation, 2014, pp. 1371–1376.

[10] K. Klausen, T. Fossen, T. Johansen, A. Aguiar, Cooperative path-following for multirotor UAVs with a suspended payload, in: IEEE Conference on Control Applications, 2015, pp. 1354–1360.

[11] D. Mellinger, M. Shomin, N. Michael, V. Kumar, Cooperative grasping and transport using multiple quadrotors, Distributed Autonomous robotic System 83 (2013) 545–558.

[12] N. Michael, J. Fink, V. Kumar, Cooperative manipulation and transportation with aerial robots, Autonomous Robots 30 Issue 1 (2010) 73–86.

[13] M. Farina, A. Perizzato, R. Scattolini, Application of distributed predictive control to motion and coordination problems for unicycle autonomous robots, Robotics and Autonomous Systems 72 (2015) 248–260.

[14] M. Farina, G. Betti, L. Giulioni, R. Scattolini, An approach to distributed predictive control for tracking–theory and applications, Transactions on Control Systems Technology 22 Issue 4 (2014) 1558–1566.

[15] B. Stevens, F. Lewis, Aircraft Control and Simulation, 2nd Edition, Mechanical Engineering, Wiley-Interscience, 2003.

[16] F. Udwadia, P. Phohomsiri, Explicit Poincaré equations of motion for general constrained systems, part 1 analytical results, Mathematical, Physical and Engineering Sciences 463 Issue 2082 (2007) 1421–1434.

[17] H. Nguyen, Constrained control of uncertain, time-varying, discrete-time systems: an interpolation-based approach, Lecture Notes in Control and Information Sciences, Springer International Publishing, 2014.

[18] D. de Falco, E. Pennestrí, L. Vita, Investigation of the influence of pseudoinverse matrix calculations on multibody dynamics simulations by means of the Udwadia-Kalaba formulation, Journal of Aerospace Engineering 22 Issue 4 (2009) 365–372.

[19] R. Mahony, V. Kumar, P. Corke, Multirotor aerial vehicles: modeling, estimation, and control of quadrotor, Robotics & Automation Magazine 19 Issue 3 (2012) 20–32.

[20] G. Oriolo, A. D. Luca, M. Vendittelli, Wmr control via dynamic feedback linearization: design, implementation, and experimental validation, Transactions on Control Systems Technology 10 Issue 6 (2002) 835–852.

[21] S. Rakovic, E. Kerrigan, K. Kouramas, D. Mayne, Invariant approximations of the minimal robust positively invariant set, Transactions on Automatic Control 50 Issue 3 (2005) 406–410.

[22] U.S. Military Specification MIL-F-8785C (November 1980).

[23] U.S. Military Handbook MIL-HDBK-1797 (December 1997).